AN ELECTROANALYTICAL STUDY OF ELECTRODE REACTIONS ON CARBON ANODES DURING ELECTROLYTIC PRODUCTION OF ALUMINUM

Hongmin Zhu and Donald R. Sadoway

Department of Materials Science and Engineering
Massachusetts Institute of Technology
Cambridge, Massachusetts 02139-4307

Abstract

In connection with the electrolytic production of aluminum the anodic reactions have been studied on carbon microelectrodes by voltammetry and chronoamperometry. Anode gases have been analyzed by gas chromatography on-line during controlled-potential electrolysis in a laboratory-scale aluminum reduction cell. When the voltage exceeds a critical value (about 3 V *vs* Al/Al^{3+}), the cell current drops precipitously. We attribute this to the formation of a highly resistive film on the surface of the anode. The existence of this putative film was shown to be strictly potential dependent - the film could be formed and removed at will by regulation of applied potential. The rate of PFC generation was found to vary with the magnitude of the anodic overpotential. A PFC reduction strategy that takes into account the design of the power supply is proposed.

Introduction

In the primary production of aluminum by the Hall-Héroult process, a cell malfunction known as the anode effect results in the generation of the perfluorocarbons (PFCs) CF_4 and C_2F_6 [1]. Owing to the high global warming potentials of these gases [2] and the fact that, in the U.S., aluminum smelting is the number one point source of PFC emissions, the Environmental Protection Agency and the primary aluminum producers have established the Voluntary Aluminum Industrial Partnership (VAIP) with the goal of substantially reducing PFC emissions [3]. To gain a better understanding of the mechanism of PFC generation, VAIP has undertaken two projects: (1) measurements of PFC emissions from industrial smelters [4], and (2) basic research into the attendant electrochemistry. The latter is the substance of the present article.

Previous work in this laboratory had shown that, in conformity with industrial data, PFCs are generated only when the cell goes on anode effect [5]. Furthermore, time-resolved data taken by Kimmerle *et al*. on industrial cells [6] and by Nissen and Sadoway on laboratory-scale cells [5] confirm that by far the highest PFC levels are attained during the first several minutes after the cell goes on anode effect. Clearly, any plan to reduce emissions needs to address this fact. Accordingly, the present investigation was directed at the underlying kinetics of PFC generation, more specifically the nature of the reactions at the electrode. The fundamental electrochemistry was studied by cyclic voltammetry and chronoamperometry. Subsequently, controlled-potential electrolysis with analysis of anode gas was performed. This article reports the results of these experiments and speculates on the mechanistic features of the reactions occurring on the anode at various potentials. In addition, the role of the power supply in sustaining undesirable PFC generation is addressed.

Experimental

The cell design was largely identical to that used previously in this laboratory [5,7]. Electrochemical measurements were made with a potentiostat (Solartron Electrochemical Interface, model 1287, Allentown, PA) controlled by a personal computer running Corrware (Scribner Associates, Southern Pines, NC). The working electrode was made of either a graphite or a glassy carbon rod, about 2 to 3 mm in diameter, shrouded by BN, so that about 10 mm in length was exposed to the melt and electrochemically active. The molybdenum crucible served as the counter electrode. The reference electrode was Al/AlF_3 based upon the design patented by Sadoway [8,9].

For the analysis of anode gas during the electrolysis, a tubular anode was used [7]. The outer vertical surface is insulated with BN; hence, only the inside walls (8 mm in dia., 10 mm height) contact the electrolyte. Anode gas was drawn through an alumina tube from the chamber formed above the melt “inside” the electrode. Gas analysis was performed by gas chromatograph (Model M200 Dual Gas Analyzer, MTI Analytical Instruments, Fremont, CA). The electrolyte was prepared from reagent-grade

chemicals: AlF_3 (98%), CaF_2 (99%) and Na_3AlF_6 (97%) dried at 500°C under Ar flow for about 12 hours and pre-melted before being introduced into the reduction cell. Prior to cell testing, melts were subjected to pre-electrolysis to rid them of impurities. All experiments were conducted at a temperature of 975ºC.

Results and Discussion

Cyclic Voltammetry

Cyclic voltammetry was performed on melts doped with alumina. Because the technique is conducted with a microelectrode and relies upon depletion of the electroactive species on a time scale comparable to that of the voltage sweep, it is necessary to fix the alumina concentration at a value much lower than is typically encountered in industrial operations. In this set of experiments, alumina levels ranged from 0.01 wt % to 0.60 wt %. The solvent was 84 wt % Na_3AlF_6 - 11 wt % AlF_3 - 5 wt % CaF_2. Figure 1 shows the behavior of a melt containing 0.01 wt % Al_2O_3 on a graphite electrode at a sweep rate of 100 mV s^{-1}. On the forward (anodic) sweep, peaks are evident at 1.8 V, 3.4 V, and 4.3 V. Repeatedly, on the reverse scan nothing measurable was found in the way of a cathodic peak, indicating that the electrode process is highly irreversible. Actually, the voltammogram of the reverse scan is rather similar to that of forward scan. We attribute the rise in current at 1.8 V to the discharge of oxide species, since the potential is not extreme enough to support the discharge of fluoride: the lowest potential for PFC evolution is 2.5 V for CF_4. We suspect that the peaks at 3.4 V and 4.3 V are related to the discharge of fluoride.

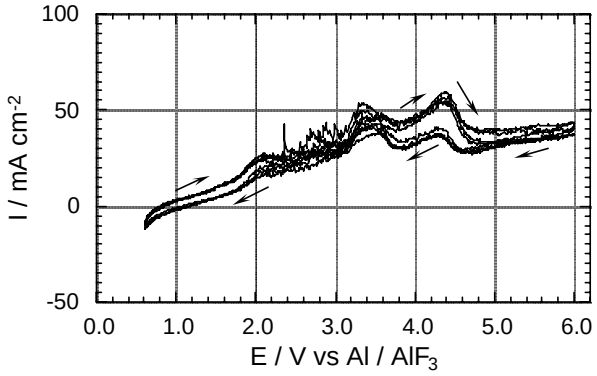

Fig. 1 Cyclic voltammogram of 0.01 wt% Al_2O_3 melt. Graphite electrode, v = 100 mV s^{-1}.

Figure 2 is a voltammogram of a melt containing 0.15 wt % alumina. As expected, because the concentration of alumina is substantially higher than it is in Figure 1, the magnitude of the anodic current of the first peak is higher. Fluctuations in current over the potential interval from 1.8 V - 3.0 V are likely caused by gas-bubble evolution at the electrode surface. At 3.0 V the current falls sharply. At 4.0 V a weak current peak is observed. At higher potentials the current drops to a very low value, ~10 mA cm^{-2}. All features of the voltammogram are reproducible on the reverse scan. Figure 3 compares the forward and reverse scans of the same melt at different sweep rates and shows that there is little variation. Predictably, the only effect the sweep rate appears to have on the voltammogram is to change the oscillation frequency of the current – at slow sweep rates, there are more oscillations and they appear more closely spaced.

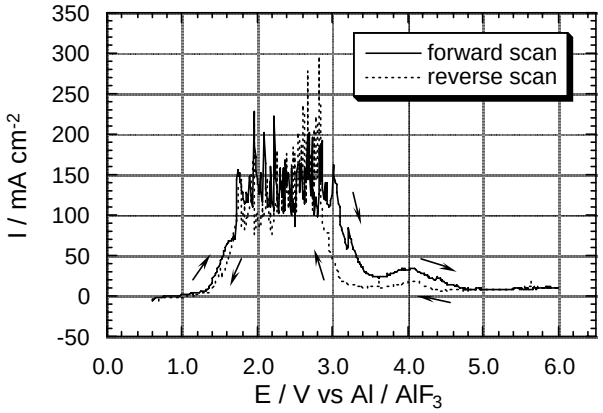

Fig. 2 Cyclic voltammogram of 0.15 wt% Al_2O_3 melt. Graphite electrode, v = 100 mV s^{-1}.

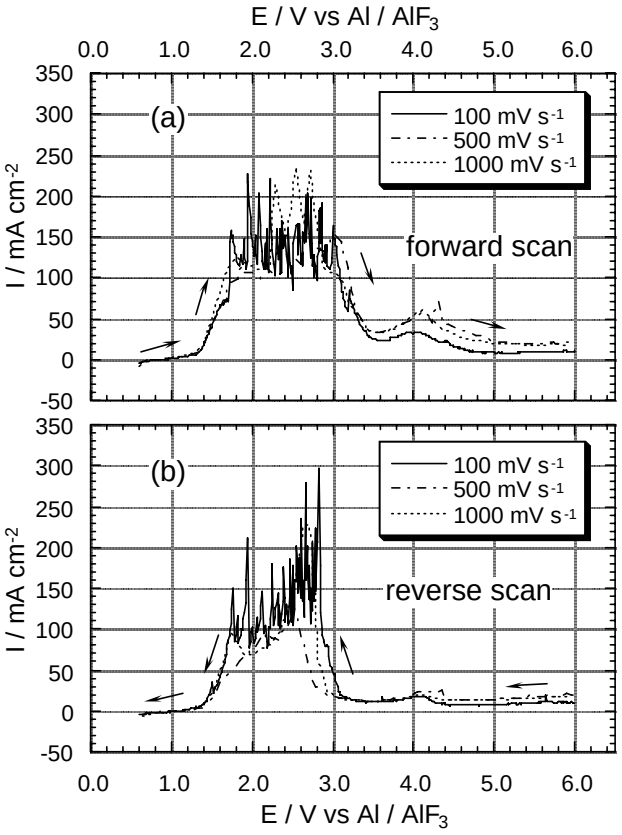

Fig. 3 Cyclic voltammetry of 0.15 wt% Al_2O_3 melt at different sweep rates. Forward and reverse scans depicted separately.

Figure 4 is the voltammogram of a melt containing 0.25 wt % alumina. The potential was swept over an exceptionally wide range – out to 14.0 V. As above, the current rises with potential up to about 3.0 V at which point there is a distinct decrease in current. What is surprising is that beyond 3.0 V, the current remains low, all the way out to 14.0 V. With the exception of a tiny peak at 4.0 V there is no evidence of faradaic activity on a

par with that observed below 3.0 V. On the reverse sweep, there is no cathodic activity (as above), and the anodic peak at 3.0 V is retraced with some offset to more cathodic potentials (~2.8 V).

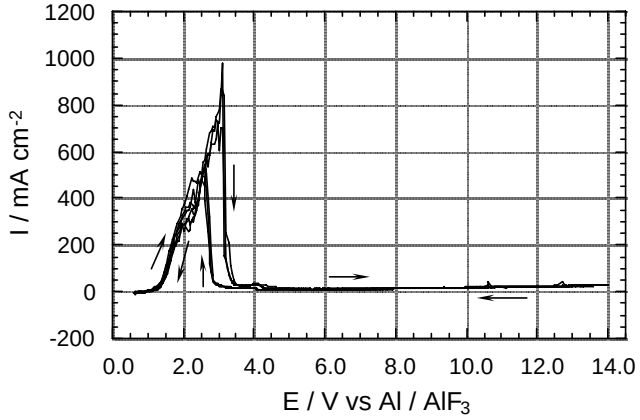

Fig. 4 Cyclic voltammogram of 0.25 wt% Al_2O_3 melt. Graphite electrode, v = 500 mV s^{-1}.

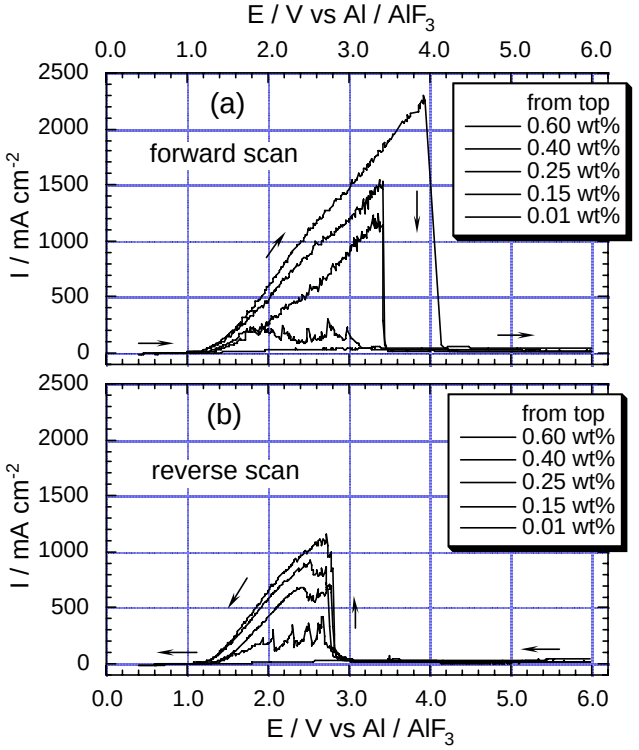

Fig.5 Cyclic voltammetry of various melts. Forward and reverse scans depicted separately. Graphite electrode, v = 100 mV s^{-1}.

Figure 5 shows the effect of alumina concentration in a set of voltammograms all taken at the same sweep rate of 100 mV s^{-1}. The current of the first wave starting at 1.2 V increases with alumina concentration which is consistent with the assignment of this peak to the discharge of oxide. The elementary process is in fact the oxidation of O^{2-} which is assumed to be present as part of an oxyfluoro-anionic species. At all alumina concentrations the current falls at intermediate potentials (3.0 - 4.0 V) and remains low even as potential increases beyond 4.0 V. There appears to be some correlation between the potential at which the current drops off (we call this the *critical potential*, E_C) and the alumina concentration: E_C rises with alumina concentration. However, on the reverse sweep, the potential at which current rises (we call this the *recovery potential*, E_{RC}) shows no dependence on alumina concentration.

Chronoamperometry

Chronoamperometry involves stepping the potential on the working electrode from rest potential value and measuring the current between the working and counter electrodes. Figure 6 shows chronoamperometric traces taken at various potentials for a sample containing 0.2 wt % alumina. A trend similar to that seen in the sweep voltammetry is observed, i.e., current increases with potential up to about 3.0 V and then falls abruptly at more extreme potentials. This is summarized in Figure 7 which plots the average current sampled from the chronoamperometric traces as a function of applied potential. On the same plot are the data from linear sweep voltammetry. While there are modest differences between the behaviors of graphite and glassy carbon electrodes, for each material the two techniques give identical results. This, together with the fact that the linear sweep voltammogram does not depend on sweep rate, indicates that the kinetics of the electrode process must be controlled by an interfacial step and not by mass transfer.

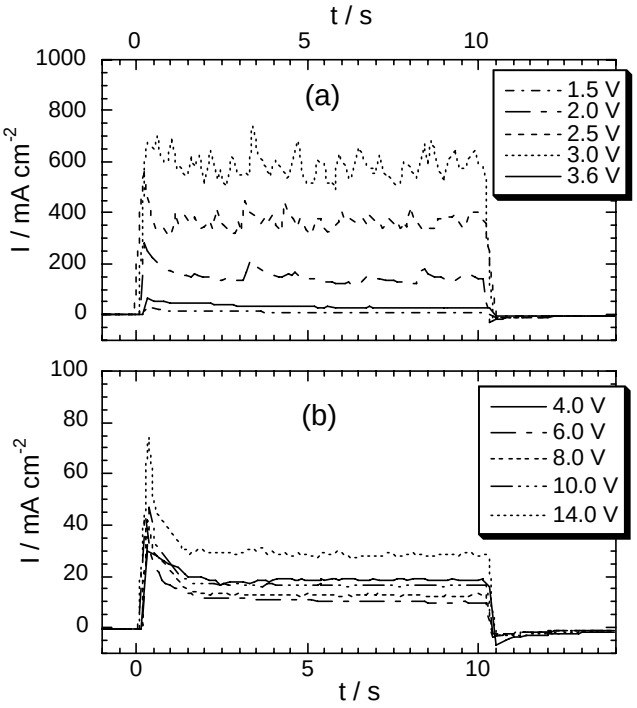

Fig. 6 Stepped – potential chronoamperometry of 0.2 wt% Al_2O_3 melt. Graphite electrode.

Gas Analysis During Controlled-Potential Electrolysis

The close correspondence between voltammograms measured by swept-potential and stepped-potential techniques indicates that the electrode reaction rate is dependent mainly upon the

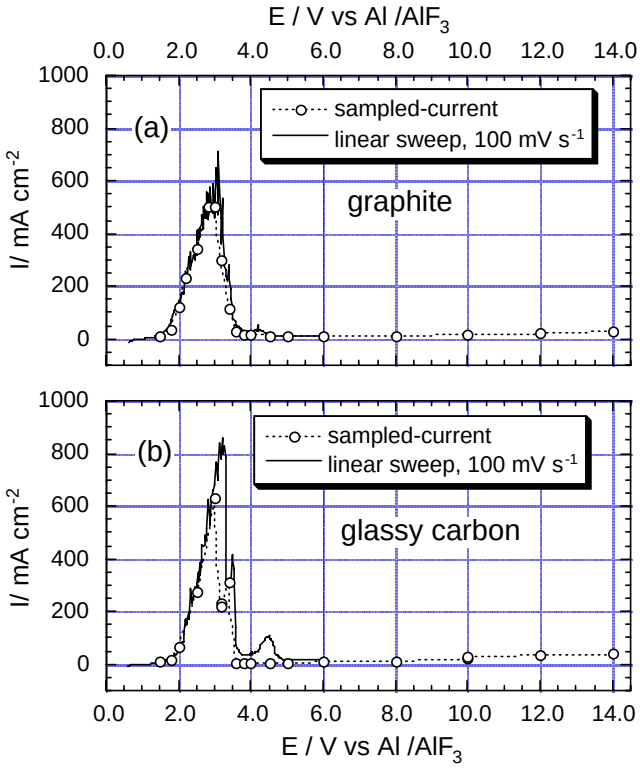

Fig. 7 Linear sweep voltammogram and sampled-current voltammogram of melt containing 0.2 wt% Al_2O_3.

electrode potential; hence, controlled-potential electrolysis combined with chemical analysis of the gas produced at the anode should prove to be insightful. Such experiments were conducted using a tubular anode in a cell described previously [7]. Simultaneously, the anode gas was analyzed before, during, and after application of the potential. Figure 8 displays the data for a potential step of 4.0 V in a melt containing alumina at a concentration of 0.1 wt %. Trace (a) shows the potential step and the current response, while (b) and (c) show how the concentration of CO, CO_2, CF_4, and C_2F_6 vary with time in the anode chamber. Apart from carbon monoxide, which is always expected to be present at the temperature of the experiment (975°C) due to the Boudouard reaction,

$$CO_2 + C = 2\,CO, \qquad (1)$$

all other gases were detected only when current passed through the cell. Furthermore, their concentrations fell to zero when current ceased to flow through the cell. We assume, therefore, that the change of gas composition during electrolysis is due to faradaic processes occurring in the cell. In another words, the change in composition should be governed by the rate of the electrode reaction that generates gases. Measurements were carried out for different potential steps up to 14.0 V. In all experiments no peaks other than those of N_2, O_2, CO, CO_2, CF_4, and C_2F_6 were detected.

Figure 9 summarizes the results of many such experiments by plotting the average values of current and gas concentration as functions of applied potential. The melt had an estimated alumina level of < 0.1 wt% Al_2O_3 and had been treated by pre-electrolysis.

In this figure, C_{CO} is the concentration of CO corrected by subtraction of the nonfaradaic baseline value. Over the entire range of potential, CO is the biggest component of the anode gas. Indeed, the shape of the CO concentration history mimics that of the cell current. At low potentials (< 2.8 V) CO_2 levels are comparable to those of CO ($C_{CO} / C_{CO_2} \approx 4$); at higher potentials CO_2 levels drop significantly. CF_4 and C_2F_6 were detected at potentials exceeding 2.8 V. At high potentials (>5.0 V), the concentration of CF_4 is comparable to that of CO ($C_{CO} / C_{CF_4} \approx 2.5$), and the concentration of C_2F_6 is much lower than that of CF_4 ($C_{CF_4} / C_{C_2F_6} \approx 50$).

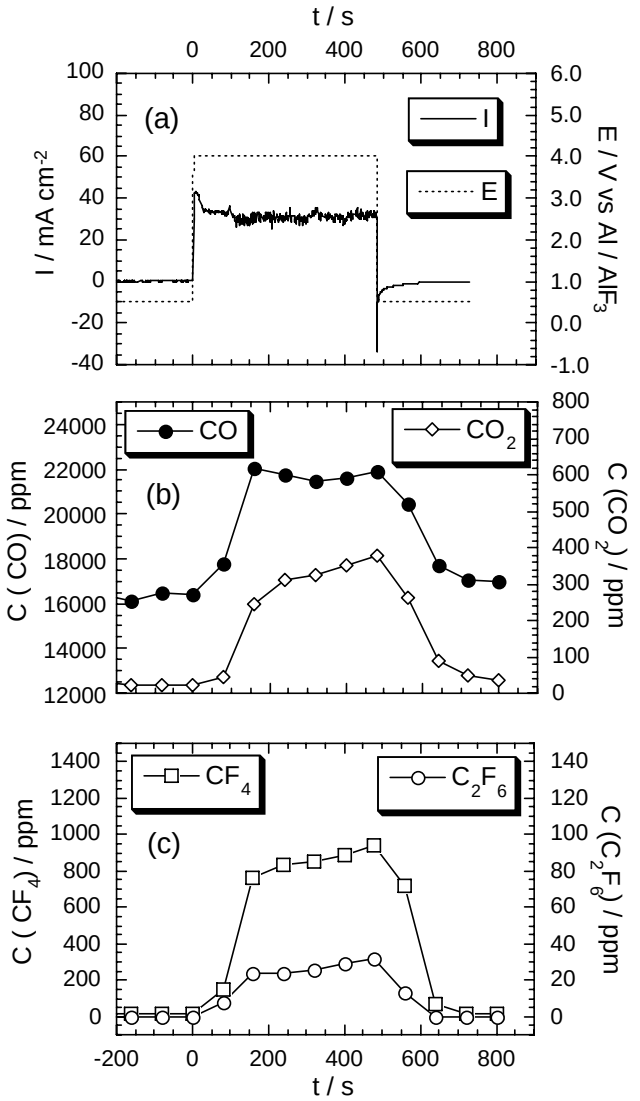

Fig. 8 Current response and anode gas composition during potential-controlled electrolysis (C_{Al2O3} < 0.1%).

Figure 10 is similar to Figure 9; however, in this case the melt contained higher amounts of alumina ($C_{Al_2O_3} \approx 0.2$ wt %) and had not been treated by pre-electrolysis. Associated with the higher oxide concentration is a higher cell current as well as higher concentrations of CO and CO_2 at low potentials. As above, CF_4 was detected only at potentials exceeding 2.8 V. Compared to the

values reported above, the measured

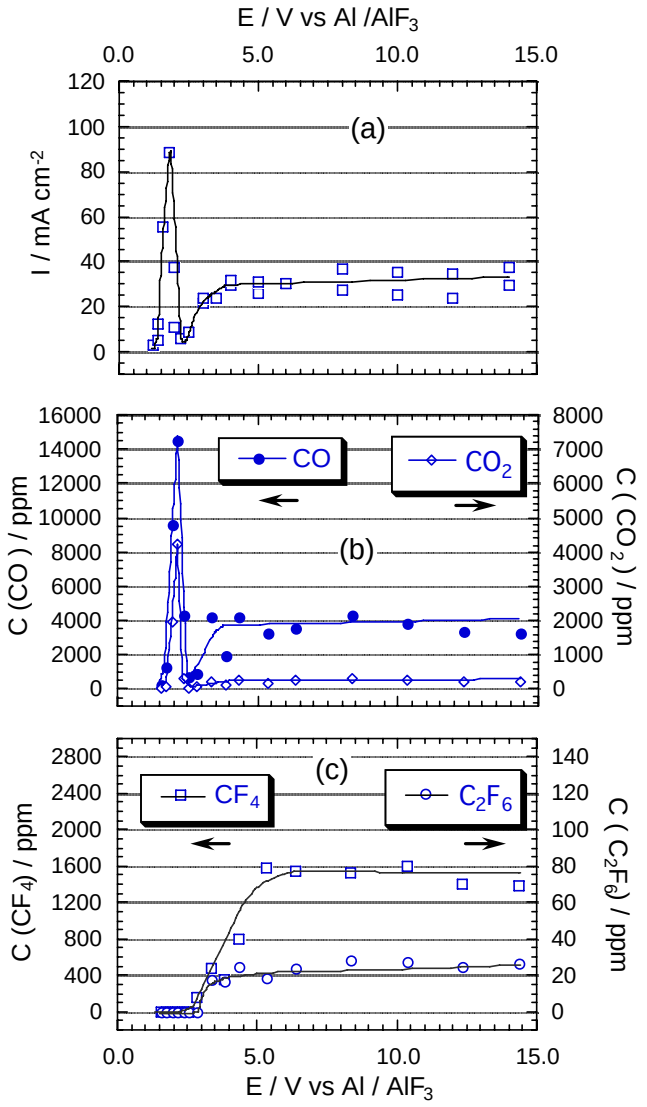

Fig. 9 Potential dependence of current and anode gas composition during potential-controlled electrolysis (C_{Al2O3} < 0.1%).

concentrations of CO and CO_2 were higher, the concentration of CF_4 was lower, and the concentration of C_2F_6 was below the limit if detection (< 1 ppm). At high potentials (E > 5.0 V) the current increases very slightly with increases in potential. In Figure 11 the variation in gas composition is plotted against potential. Clearly, in the high-potential region the emission rate of the gases obeys an expression of the form

$$ln\, \boldsymbol{C} = \alpha + \beta \boldsymbol{E} \qquad (2)$$

This equation is equivalent to the formula given by Nissen and Sadoway [5] for the emission rate of CF_4:

$$r_{CF_4} = a\, exp\,(b\, E\,) \qquad (3)$$

They reported the coefficient b to be 0.331 V^{-1} based upon controlled-current electrolysis. From the slope of the line in Figure 11, β was calculated to be 0.325 V^{-1} for CF_4, in excellent agreement with the value of b. This high degree of similarity is rather surprising, considering the big differences in the conditions of the two experiments, i.e., electrode surface area, volume of the anode chamber, the method of power delivery, etc.

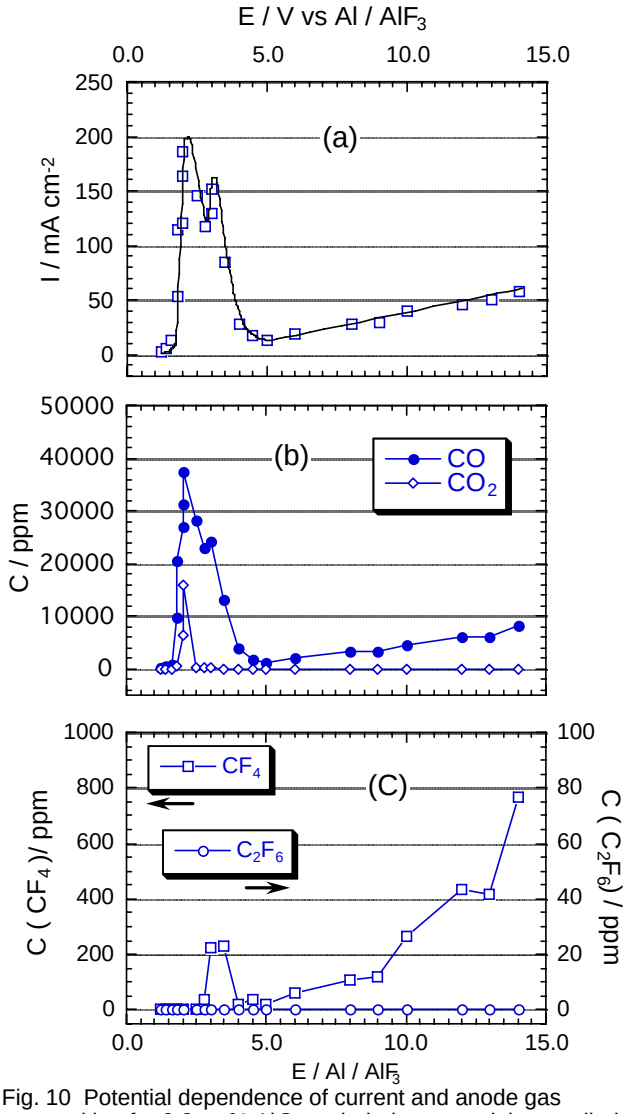

Fig. 10 Potential dependence of current and anode gas composition for 0.2 wt % Al_2O_3 melt during potential-controlled electrolysis.

Anodic Reactions and the Anode Effect

The results of the anode gas analysis clearly indicate that the first faradaic process, occurring at potentials exceeding 1.2 V, is the oxidation of oxide with the formation of CO and CO_2. At more extreme potentials (>2.8 V) we observe the oxidation of fluoride with the formation of CF_4 as expressed by several rather weak peaks. The relationship between the oxide and fluoride peak heights is in stark contrast to the concentrations of the two species. In all our experiments the oxide (Al_2O_3) concentration was very low (<0.25 wt %): the melts were essentially fluorides doped with a tiny amount of alumina. In spite of this, the fluoride peaks are small relative to the oxide peak. One explanation is that at potentials capable of supporting PFC evolution the anode is

covered by a film that acts as an electrical insulator. On the basis of this work alone not much can be said about the chemistry of the film. However, in an analogous system, molten KF-HF, Imoto *et al.* [10] and Bai *et al.* [11] have suggested that the formation of a "CF" film will inhibit the electrode process and contribute to anode effect. Our results are consistent with the formation of an insulating film at intermediate potentials which, in turn, inhibits the electrode process at more extreme potentials.

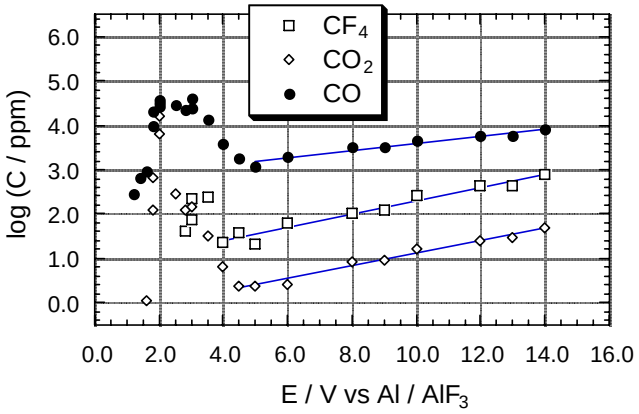

Fig. 11 Anode gas emission rates as a function of applied potential (0.2 wt % Al_2O_3).

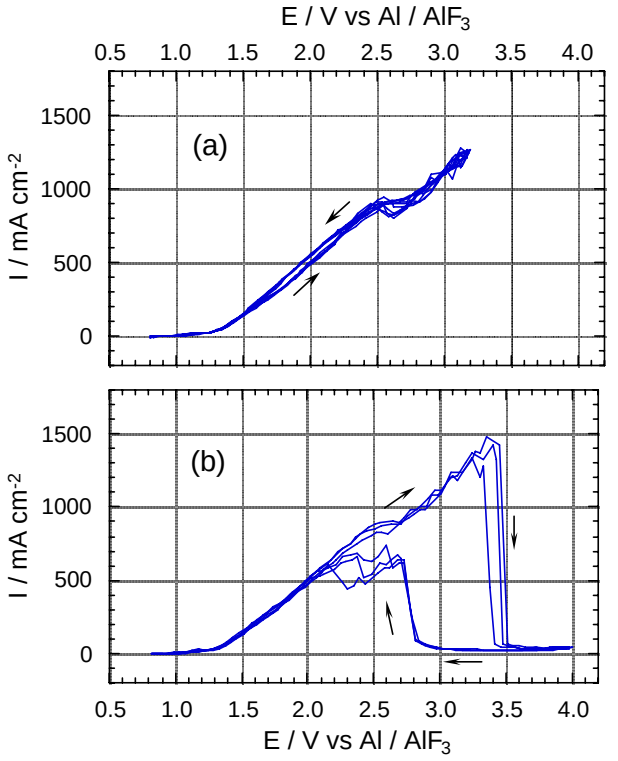

Fig. 12 Cyclic voltammogram of 0.40 wt% Al_2O_3 melt. Graphite electrode, v = 500 mV s^{-1}.

Further support can be found in the following.

(1) In some of our experiments the anode was vertically disposed (the inside wall of a graphite tube) which made it impossible to accumulate gas on its surface, yet the cell went on anode effect.

(2) The recovery potential, E_{RC}, does not depend on the oxide concentration. Thus, we expect the resistant film to be a fluorocarbon compound – formed when the discharge of fluoride ion occurs and sustained only at high potentials.

Figure 12 is a set of cyclic voltammograms displaying the key effect of the electrode potential on the anode effect. The voltammogram (a) is fully retraceable when the reverse potential is lower than the critical potential. The anode effect occurs when the potential exceeds 3.4 V (b), and the electrode becomes faradaically active again when the potential is swept back to potentials lower than 2.8 V. It is as though the shift to less anodic potential promotes active stripping of the putative resistive film, thereby rendering the electrode electrochemically active. Perhaps the hysteresis seen in (b) is evidence of activation barriers associated with film formation on the anodic sweep and with film removal on the return sweep.

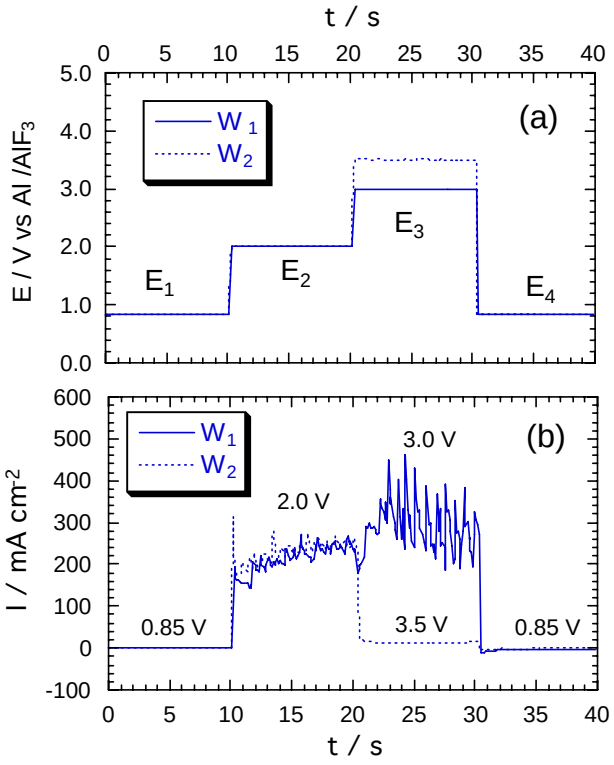

Fig. 13 Current response of square potential wave. C_{Al2O3} - 0.15 wt%, graphite electrode.

Figure 13 compares the current responses to two different potential waveforms. In both cases, the electrode was held at 4 potentials, E_1, E_2, E_3, and E_4, for ten seconds each, and the current was monitored. E_1 and E_4 were set to the rest potential of the electrode, 0.85 V, and E_2 was set to 2.0 V. The only difference between the two waveforms is in the value of E_3: 3.0 V in one case and 3.5 V in the other. These potentials were chosen to straddle the critical potential, E_C. The current response for both waveforms is identical at E_1, E_2, and E_4. There is a pronounced difference at E_3. Figure 14 shows this effect even more vividly. In this case the potential waveform is repeated: E_1 = 0.85 V, E_2 = 2.0 V, E_3 = 5.0 V, and E_4 = 3.0. It is clear that when the electrode potential is set at 5.0 V an insulating barrier blocks current flow.

The effect is reversed as soon as the potential drops to 3.0 V, which is below the critical potential. These current responses are reproducible for many cycles.

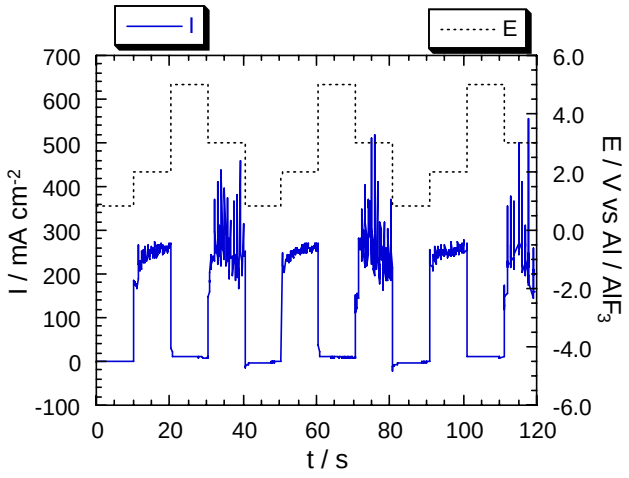

Fig. 14 Current response of square potential wave. C_{Al2O3} - 0.15 wt%, graphite electrode.

Possible Way to Reduce the AE and PFC Generation

Once the electrode goes on anode effect, the current will fall quickly, and the electrode will follow the polarization curve shown in Figures 4, 5, and 7. In the high-potential region the current rises slightly with increasing potential, and the fraction of PFC in the anode gas increases. This tendency can be seen in Figures 9 and 10. The results of measurements made in aluminum smelters [6] and in laboratory-scale cells [5] indicate that the most intense period of PFC emission is the first moments of high voltage immediately following the onset of the anode effect. Accordingly, we propose the following without any regard for instant practicality: a minimalist approach to power source design. If it were possible to ensure that the power source be incapable of sustaining the required current at elevated voltages, say in excess of 5 V, then the cell would effectively be prevented from going on anode effect. The authors recognize that the plurality of anodes in a single cell make this proposal nontrivial to implement. However, in laboratory cells driven by power supplies that furnish voltages no greater than 10 V, for example, when the cell tries to go on anode effect, the voltage rises from its normal value of about 4 V to a little over 10 V at which point the current starts to fall. Since faradaic yield is related to current, PFC production is stunted by the decrease in current and simultaneous failure of the voltage to rise beyond 10 V. If this feature could be designed into the power delivery systems of industrial smelters, the intense period of PFC generation immediately following the onset of anode effect might be averted.

Acknowledgments

The authors gratefully acknowledge the assistance of the Aluminum Association PFC Task Force, including Dr. Jerry Y. Marks (Alcoa), Mr. Robert P. Strieter (Aluminum Association) for their technical guidance and for providing industrial materials and reagents; and Dr. Eric J. Dolin of the U.S. Environmental Protection Agency for his office's support of basic research. Financial support for this investigation was provided jointly by the Aluminum Association and the U.S. Environmental Protection Agency, Climate Protection Division. The Massachusetts Institute of Technology contributed matching funds from the MacVicar Foundation in the form of a faculty fellowship (for DRS).

References

1. A.T. Tabereaux, "Anode Effects, PFCs, Global Warming, and the Aluminum Industry," JOM, 42 (11) (1994), 30-34.
2. Radiative Forcing of Climate Change: Summary for Policymakers, the 1994 report of the Scientific Assessment Working Group of the Intergovernmental Panel on Climate Change (IPCC), World Meteorological Organization, and the United Nations Environment Program.
3. E.J. Dolin, "PFC Emissions Reductions: The Domestic and International Perspective," Light Metal Age, (2) (1999), 56-67.
4. B.P Leber, A.T. Tabereaux, J. Marks, B. Lamb, T. Howard, R. Kantamaneni, M. Gibbs, V. Bakshi and E.J. Dolin "Perfluorocarbon (PFC) Generation at Primary Aluminum Smelters," Light Metals 1998, B.J. Welch, editor, (Warrendale PA: TMS), 1998, pp. 277-285.
5. S.S. Nissen and D.R. Sadoway, "Perfluorocarbon (PFC) Generation in Laboratory-Scale Aluminum Reduction Cells," Light Metals 1997, S.K. Das, editor, (Warrendale PA: TMS), 1997, pp. 159-164.
6. F.M. Kimmerle, G. Potvin, and J.T. Pisano, "Measured versus Calculated Reduction of the PFC Emissions from Prebaked Hall-Héroult Cells," Light Metals 1998, B.J. Welch, editor, (Warrendale PA: TMS), 1998, pp. 165-175.
7. H. Zhu and D.R. Sadoway, "The Electrode Kinetics of Perfluorocarbon (PFC) Generation," Light Metals 1999, C.E. Eckert, editor, (Warrendale PA: TMS), 1999, pp. 241-246.
8. D.R. Sadoway, inventor, Massachusetts Institute of Technology, assignee, "Aluminum Reference Electrode," U.S. patent no. 4,764,257, August 16, 1988.
9. J.N. Hryn and D.R. Sadoway, "Cell Testing of Metal Anodes for Aluminum Electrolysis," Light Metals 1993, S.K. Das, editor, (Warrendale PA: TMS), 1993, pp. 475-483.
10. H. Imoto, K. Ueno and N. Watanabe, "A Study on the Anode Effect in KF-2HF System. III," Bull. Chem. Soc. Jpn., 51 (10) (1978), 2822-2825.
11. L. Bai and B.E. Conway, "Electrochemistry of Anodic Fluoride Gas Evolution at Carbon Electrodes," J. Appl. Electrochem., 20(6) (1990), 925-931.